Unsteady MHD Casson Fluid Flow Past an Inclined Surface Subjected to Variable Magnetic Field, Heat Generation and Effective Prandtl Number

George Buzuzi

Abstract— **The paper reports on the influence of effective Prandtl number, aligned magnetic field, slope of the stretching channel and heat generation on unsteady MHD Casson fluid flow. The partial differential equations of momentum, temperature and concentration are converted to non-linear ordinary differential equations by introducing appropriate similarity variables. The solution of the ODE's are calculated numerically using MATLAB bvp4c solver. The role of the different parameters on the temperature, velocity, and concentration profiles are analyzed and presented in the form of graphs and tables. Finally the impact of the different parameters on the mass transfer rate, heat transfer rate and skin friction are discussed. It is revealed that lowering the inclination angle enhances the velocity and temperature profiles with opposite effect on the concentration distribution. The concentration, temperature and velocity profiles decline with enlarged values of the unsteadiness parameter. Furthermore, the velocity profile, the temperature profile at free stream, skin friction coefficient, mass transfer rate and heat transfer rate diminishes with magnified effective Prandtl number.**

Index Terms – **Casson flow, MHD, aligned magnetic field, inclined surface, effective Prandtl number.**

I. INTRODUCTION

THE field of non-Newtonian MHD flow has generated interest among several authors. Several applications in the field exists which include nuclear fuel debris treatment, solidification process of metals and MHD power generation. The study examines the unsteady MHD flow of Casson fluid past an inclined stretching sheet which is subjected to variable magnetic field and heat generation. Casson fluids are non-Newtonian fluids which exhibits solid behaviour provided yield stress is greater applied shear stress and exhibit fluid behaviour if the relationship between yield and shear stress is reversed. Koroleva and Korolev [21] discovered that blood in thin capillaries near the walls is non-Newtonian and exhibits rheological properties that can be modelled using Casson's system of differential equations. Besides blood being Casson fluid, other examples of such a fluid are fruit juice, soup, chocolate and honey.

Studies on Casson flow over stretching /shrinking surfaces, have been carried out by several researchers, who among them are, Battachrya *et al.* [7], Mukhopadhyay [27] and Nadeem *et al.* [29]. Casson fluid past a shrinking sheet was examined by Battacharya [8]. Nadeem [30] investigated Casson fluid containing nano particles subjected to convective boundary conditions. Furthermore, Pramanik [31] investigated the effect of thermal radiation on Casson fluid past a porous stretching sheet.

Dufour and thermophoresis effect on the Casson fluid is significant in this study. The mass flux triggered by temperature gradient is called thermophoresis or Soret effect and the heat flux which is triggered by concentration gradient is termed the Dufour effect. Das *et al.* [14] noted that both Soret and Dufour effects can occur simultaneously. Abreu *et al.* [4] investigated the double-diffusive effect on a flow with different boundary conditions. The impact of chemical reaction, suction, Dufour and thermophoresis of a casson fluid was investigated by Animasaun [5]. Recently, Das *et al.* [15] reported on Soret and Dufour effect on unsteady MHD flow along a flat plate in a porous medium.

The influence of thermal radiation on Casson fluid is also explored in the present study. Understanding the role of radiation heat transfer in a system is very crucial since it helps us to control the characteristics or attributes of the end product in that system. Some of the authors who reported on the effect of thermal radiation are, Seddeeck and Muguid [39], Ibrahim *et al.* [23] and Roja *et al.* [35]. Studies by Buzuzi[13], Buzuzi and Makanda [11], Mgyari [25] and Magyari and Pantokratoras [26] demonstrated the trivial effect of thermal radiation when the radiative heat flux is described by Rosseland approximation. They noticed that the effect of the thermal radiation on the fluid is the same as that of the Prandtl number which only differ in the magnitude of the impact. It was established that the solution obtained depends on the combined effect of both the radiation parameter and the Prandtl number called the effective Prandtl number instead of considering their impacts separately. This study examines the role of effective Prandtl number on Casson flow. Numerous studies have been conducted were the magnetic field was applied normal to the channel surface, a case in which the resis-

Manuscript received July 07, 2022; revised December 02, 2022;
George Buzuzi is a mathematics lecturer at Department of Mathematics and Physics, Cape Peninsula University of Technology, P O Box 1906, Belville, 7535, South Africa (phone: +27 82 971 3160; email: buzuzig@cput.ac.za).

tance to flow due to Lorentz force is minimal. However, due to limitations and variations in the geometry of surfaces upon which fluid flows, the magnetic field maybe applied at different angles. Studies on the effects of the aligned magnetic field to fluid flow have caught the attention of many researchers who include among others, Salawa and Dada [36], Acharya *et al.* [1], Sandeep and Sugunamma [37], Raju *et al.* [33], Buzuzi[13]and Buzuzi and Makanda [11]. Gopel *et al.* [18] analysed the effect of chemical reaction, Joule heating and variable magnetic field on Casson fluid. Findings were that the impact of increasing the magnetic field inclination is to raise the rate of heat transfer , strengthen the magnetic field and diminish the velocity profile.
Investigations on fluid flow past inclined surfaces have received attention of many authors who among them are Buzuzi and Makanda [11], Uddin [42], Alam *et al.* [2], Buzuzi *et al.* [12], Buzuzi *et al.* [9], Buzuzi and Buzuzi [10], Buzuzi [13] and Alam *et al.* [3]. Specifically with regard to Casson flow, Gurran *et al.* [19] investigated the influence of channel slope, radiation and chemical reaction on MHD Casson fluid. Jain and Kumari [20] reported on the role of viscous dissipation and chemical reaction on MHD Casson fluid past an inclined permeable cylindrical surface. Later, Rafique *et al.* [32] studied the Soret and Dufour effect on Casson nano-fluid past an inclined surface. The studies disclosed that increasing the flow surface inclination grows the temperature profile and reduces the velocity.

In the majority of the studies mentioned so far, researchers have investigated fluid flow involving either aligned magnetic field or inclined flow surface but not both. Recently however, a few authors have analysed the effect of both aligned magnetic field and inclined flow surface. Reddy *et al.* [34], Sivaraj and Sheremet [41], Buzuzi and Buzuzi [10], Buzuzi [13], Kumar *et al.* [22] and Buzuzi and Makanda [11] are among the few researchers who analyzed the role of both variable magnetic field and flow channel inclination. Whereas most of these researchers considered the effect of the inclination angles seperately, Buzuzi [13]and Buzuzi and Makanda [11], explored the combined effect of both aligned magnetic field and inclined surface on MHD free convective newtonian flow. The current study addresses the simultaneous effect of both inclination angles on Casson flow in contrast to Buzuzi [13], Buzuzi and Makanda [11] whose focus was on newtonian flow. Our current study puts emphasis on the impact of the effective Prandtl number and the combined effect of the inclination angles coupled with different boundary conditions which is not the case with studies by Kumar *et al.* [22].

No studies have been made so far that analyzes the impact of variable magnetic field, channel slope and effective Prandtl number on unsteady MHD Casson fluid, hence motivation for the current investigation.

The next section of the paper presents the formulation of the problem which is then followed by a section covering the method of solution. Thereafter, a section on results and discussion is provided. Finally, the last section will conclude the investigation.

II. PROBLEM FORMULATION

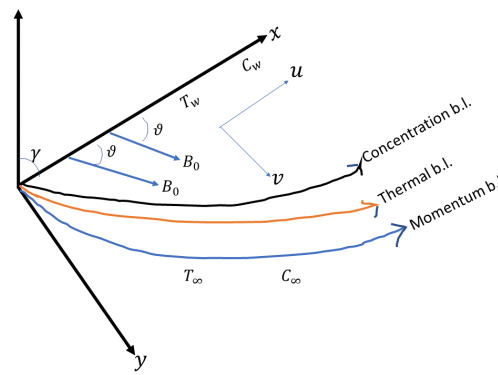

Figure 1: Flow geometry

Consider the unsteady MHD flow of viscous, incompressible, electrically conducting fluid undergoing a first order chemical reaction past an inclined sheet subjected to aligned magnetic field and heat generation. The flow geometry is depicted in Figure 1 with the $x-$axis along the slope ad the $y-$ axis directed perpendicular to it. The stretching sheet is inclined at an angle γ from the vertical. A magnetic field of uniform strength B_0 is directed at an angle ϑ to the $x-$ direction. The sheet velocity is given by $U_w(x,y) = \frac{c_1 x}{1-\omega t}$ [24] where $\omega > 0$ and the initial stretching rate $c_1 \geq 0$. The role of the magnetic field is insignificant as the Reynolds number is very small. The effects of thermophoresis and Dufour are considered significant in the current study. The Casson fluid rheological equation ([28], [6])

$$\tau_{ij} = \begin{cases} \left(2\mu_B + \sqrt{\frac{2}{\pi}}P_y\right) e_{ij} & \pi > \pi_c \\ \left(2u_B + \sqrt{\frac{2}{\pi_c}}P_y\right) e_{ij}, & \pi < \pi_c \end{cases}$$

where P_y is the fluid yield stress, μ_B is the plastic dynamic viscosity and π_c is the critical value based on the non-Newtonian model. In the present study we considers the case $\pi > \pi_c$ and $\frac{\mu}{\rho} = \mu_B/\rho\left(1+\frac{1}{\beta}\right)$. These assumptions together with the usual Boussinesq approximations, the governing equations are ([43], [15], [6]):

$$\begin{aligned} \beta\frac{\partial u}{\partial t} + \beta u\frac{\partial u}{\partial x} + \beta v\frac{\partial u}{\partial y} &= \nu\left(1+\beta\right)\frac{\partial^2 u}{\partial y^2} \\ -\frac{\beta\sigma {B_o}^2 \sin^2\vartheta}{\rho} - \beta\frac{\nu}{K}u + & \ g\beta\beta_t(T-T_\infty)\cos\gamma \\ & +g\beta\beta_m(C-C_\infty)\cos\gamma, \end{aligned} \tag{1}$$

$$\begin{aligned} \frac{\partial T}{\partial t} + u\frac{\partial T}{\partial x} + v\frac{\partial T}{\partial y} &= \alpha\frac{\partial^2 T}{\partial y^2} + \frac{Q_0(T-T_\infty)}{\rho C_p} \\ &+\frac{DK_T}{c_{st}c_p}\frac{\partial^2 C}{\partial y^2} - \frac{\mu}{\rho c_p}\left(1+\frac{1}{\beta}\right)\left(\frac{\partial u}{\partial y}\right)^2 \\ & -\frac{1}{\rho c_p}\frac{\partial q_r}{\partial y} + \frac{\sigma B_0^2 u^2}{\rho c_p}, \end{aligned} \tag{2}$$

$$\frac{\partial C}{\partial t}+u\frac{\partial C}{\partial x} + v\frac{\partial C}{\partial y}=D\frac{\partial^2 C}{\partial y^2} +\frac{DK_T}{T_m}\frac{\partial^2 T}{\partial y^2} - K_r(C-C_\infty), \quad (3)$$

where u and v are the velocities directed parallel to the x and y axes respectively. T denotes the fluid temperature, C represents the concentration of the fluid, T_m denotes the mean fluid temperature, B_0 denotes the magnetic field intensity, K_T represents the thermal diffusion ratio, g is the acceleration due to gravity, ν represents the kinematic viscosity, β_t is the thermal coefficient of expansion, β_m denotes the solutal coefficient of expansion, D represents the mass diffusivity coefficient, κ represents the thermal conductivity of the fluid, ρ is the density, c_p represents the specific heat, c_{st} denotes the concentration susceptibility, Q_0 represents the heat generation parameter and β is the Casson fluid parameter. The corresponding boundary conditions are

$$v=-v_w,\ u=U_w,\ C=C_w,\ T=T_w, \quad \text{at}\ \ \mathrm{y}=0,$$
$$T\to T_\infty,\ C\to C_\infty,\ u\to 0, \quad \text{as}\ \ y\to\infty \quad (4)$$

By using Rosseland approximation the radiant heat flux q_r is described as

$$q_r=-\frac{4\sigma^*}{3K^*}\cdot\frac{\partial T^4}{\partial y} \quad (5)$$

where K^* denotes the mean absorption coefficient and σ^* represents the Stefan-Boltzman constant. Following Shateyi *et al.* [40], T^4 was expanded using Taylor series about T_∞ and by neglecting terms of orders higher than the first degree we get

$$T^4\approx -3T_\infty^4+4T_\infty^3 T \quad (6)$$

Consequently,

$$q_r=\left(\frac{-16\sigma^* T_\infty^3}{3K^*}\right)\frac{\partial^2 T}{\partial y^2}$$

Equation (2) reduces to

$$\frac{\partial T}{\partial t}+u\frac{\partial T}{\partial x}+v\frac{\partial T}{\partial y} = \frac{\kappa}{\rho c_p}\frac{\partial^2 T}{\partial y^2}+\frac{Q_0(T-T_\infty)}{\rho C_p} +\frac{DK_T}{c_{st}c_p}\frac{\partial^2 C}{\partial y^2} - \frac{\mu}{\rho c_p}\left(1+\frac{1}{\beta}\right)\left(\frac{\partial u}{\partial y}\right)^2 +\frac{16\sigma^* T_\infty^{*3}}{3\rho K^* c_p}\frac{\partial^2 T}{\partial^2 y} + \frac{\sigma B_0^2 u^2}{\rho c_p}.$$

We introduce the following similarity variables in the equations (1) - (3) and boundary conditions (4):

$$\eta=\left(\frac{c_1}{\nu(1-\omega t)}\right)^{1/2}y,\quad \psi=\left(\frac{c_1\nu}{(1-\omega t)}\right)^{1/2}xf(\eta),$$
$$\frac{T-T_\infty}{T_w-T_\infty}=\theta(\eta),\quad \frac{C-C_\infty}{C_w-C_\infty}=\phi(\eta), \quad (7)$$

and $T_w-T_\infty=\dfrac{c_1x^2T_0}{2\nu(1-\omega t)^{3/2}}$, $C_w-C_\infty=\dfrac{c_1x^2C_0}{2\nu(1-\omega t)^{3/2}}$ (see [24]) where $f(\eta)$ denotes the dimensional stream function, $\theta(\eta)$ denotes the temperature distribution function, $\phi(\eta)$ represents the concentration distribution function, T_0 represents the reference temperature and C_0 represents the reference concentration. By substituting (7) into (1)- (3) we get the following non-dimensional, non-linear and coupled ODE's:

$$\left[\frac{1+\beta}{\beta}\right]f'''-\chi\left[\frac{\chi}{2}\eta f''+f'\right]+ff''-f'^2 -G_t\theta\cos\gamma+G_m\phi\cos\gamma -\left[Msin^2\vartheta+k_p+\chi\right]f'=0 \quad (8)$$

$$\theta''-P_{ref}\left[0.5\chi\eta\theta'+(1.5\chi-Q)\theta+2f'\theta\right] +P_{ref}\left[\left(\frac{1+\beta}{\beta}\right)E_cf''^2-f\theta'\right] +P_{ref}\left[ME_cf'^2+D_n\phi''\right]=0 \quad (9)$$

$$\frac{1}{S_c}\phi''-\left[0.5\eta\chi\phi'+1.5\chi\phi+2f'\phi-f\phi'\right] -\left[S_r\theta''-k_l\phi\right]=0 \quad (10)$$

The associated boundary conditions can be written as:

$$f(0)=S_f,\ f'(0)=1,\ \theta(0)=1,\ \phi(0)=1,$$
$$f'(\infty)=0,\ \theta(\infty)=0,\ \phi(\infty)=0, \quad (11)$$

where the prime ($'$) represents differentiation with respect to η where $P_{ref}=3P_r/(3+4R)$ is the effective Prandtl number, $P_r=\nu/\alpha$ denotes the Prandtl number, $R=4\rho T_\infty^3/\kappa K$ is the radiation parameter, $\chi=\omega/c_1$ represents the unsteadiness parameter, $k_p=\nu(1-\omega t)/Kc_1$ denotes the permeability parameter, $S_c=\nu/D$ is the Schmidt number, $D_n=K_TD(C_w-C_\infty)/c_1c_{st}c_p\nu(T_w-T_\infty)$ represents the Dufour number, $S_r=DK_TT_0/\nu C_0T_m$ is the Soret number, $Q=Q_0/\rho c_pc_1$ is the heat generation parameter, $G_t=g\beta_t(T_w-T_\infty)(1-\omega t)^2/c_1^2x$ represents the local thermal Grashof number, $G_m=g\beta_m(C_w-C_\infty)(1-\omega t)^2/c_1^2x$ denotes the local solutal Grashof number, $M=\sigma B_0^2(1-\omega t)/\rho c_p$ is the magnetic parameter, $S_f=v_w\sqrt{c_1/\nu}$ represents the suction or blowing parameter and $k_l=K_r(1-\omega t)/c_1$ denotes the chemical reaction parameter. The three important physical quantities of interest in this investigation are the local skin friction, the heat transfer rate and the mass transfer rate. The expressions for the local skin friction takes the form

$$Re_x^{1/2}C_f=\left(\tfrac{1+\beta}{\beta}\right)f''(0), \quad (12)$$

where C_f represents the skin friction coefficient. The heat transfer rate is written as

$$Re_x^{-1/2}Nu_x=-\theta'(0), \quad (13)$$

where Nu_x represents the local Nusselt number. The mass transfer rate takes the following form

$$Re_x^{-1/2}Sh_x=-\phi'(0), \quad (14)$$

where Sh_x denotes the local Sherwood number.

III. METHOD OF SOLUTION

The non-linear system of ODE's (8) - (10) together with the associated boundary conditions (11) are solved using MATLAB package **bvp4c**. Let

$$\frac{df}{d\eta} = y_2,$$

$$\frac{d^2f}{d\eta^2} = y_3,$$

$$y_3' = \frac{\left[f'^2 + 0.5\chi\eta y_3 + (Msin^2\vartheta + k_p + \chi)y_2\right]}{\left(1+\frac{1}{\beta}\right)} - \frac{\left[ff'' + G_t\cos\gamma y_4 + G_m\cos\gamma\ y_6\right]}{\left(1+\frac{1}{\beta}\right)},$$

$$y_5$$

$$y_5' = \frac{P_{ref}\left[0.5\chi\eta y_5 + (1.5\chi - Q)\,y_4 + 2y_2y_4\right]}{1 - D_nS_cS_rP_{ref}} - \frac{P_{ref}\left[y_1y_5 - (1+\frac{1}{\beta})E_cy_3^2 - ME_cy_2^2\right]}{1 - D_nS_cS_rP_{ref}} - \frac{P_{ref}D_nS_c\left[0.5\chi\eta y_7 + 1.5\chi y_6 - k_ly_6\right]}{1 - D_nS_cS_rP_{ref}} + \frac{P_{ref}D_nS_c\left[2y_2y_6 - y_1y_7\right]}{1 - D_nS_cS_rP_{ref}}$$

$$\frac{d\theta}{d\eta} = y_7,$$

$$y_7' = \frac{S_c\left[0.5\chi\eta y_7 + (1.5\chi + k_l)\,y_6\right]}{1 - D_nS_rP_{ref}S_c} - S_cS_rP_{ref}\frac{[0.5\chi\eta y_5 + (1.5\chi - Q)y_4) - 2y_2y_4]}{1 - D_nS_rP_{ref}S_c} - \frac{S_cS_rP_{ref}\left[y_1y_5 + (1+\frac{1}{\beta})E_cy_3^2 + ME_cy_2^2\right]}{1 - D_nP_{ref}S_cS_r} \tag{15}$$

with the following corresponding conditions:

$$y_1(0) - S_f,\ y_2(0) - 1,\ y_2(7),\ y_4(0) - 1,\ y_4(7),\ y_6(0) - 1,\ y_6(7), \tag{16}$$

Choosing $\eta_{max} = 7$ guarantees that accurate values of all the asymptotic numerical solutions are obtained. Further detail on the method of solution is found in [40] and references therein.

IV. RESULTS AND DISCUSSION

The impact of chemical reaction, effective Prandtl number, aligned magnetic field and heat generation on unsteady MHD flow is reported. The impact of effective Prandtl number (P_{ref}), magnetic field inclination angle (ϑ), flow field inclination angle (γ), magnetic parameter (M), thermal Grashof number (G_t), solutal Grashof number (G_m), Dufour parameter (D_n), Soret parameter (S_r), chemical reaction parameter (k_l), heat generation parameter (Q), suction or blowing parameter (S_f), unsteadiness parameter (χ), Eckert number (E_c), and Casson fluid parameter (β) on the concentration profile, temperature profile, velocity profile, heat transfer rate, mass transfer rate, and skin friction are displayed in tabular and graphical form.

To validate the accuracy of the present numerical solution a comparison was made between the current outcome and results reported by Mansour *et al.* [24], Sharidan *et al.* [38] and Mukhopadhyay *et al.* [28] for unsteady Newtonian flow related to the skin friction coefficient $-f''(0)$ (see Table 1). An excellent agreement is found to exist.

Figures 2, 11 and 19 portray the influence of the unsteadiness parameter on the profiles of the velocity, temperature and concentration respectively. The figures reveal that the momentum, thermal and concentration profiles diminish when the unsteadiness parameter is enhanced. It is observed, however that the impact of the unsteadiness parameter on the concentration distribution is reversed for $\chi > 0.4$. The reduction in the temperature profile with enlarged χ is a consequence of reduced heat transfer from the stretching sheet to the fluid. The transition from laminar to turbulent flow is inhibited by the reduction of the boundary thickness as χ is magnified.

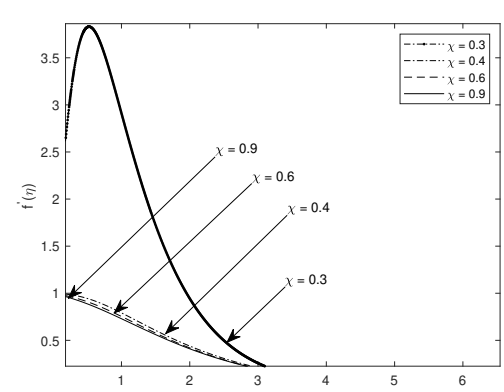

Figure 2: The influence of χ on the velocity profile for $P_{ref} = 2,\ M = G_t = G_m = S_f = 1,\ \beta = 0.2,\ \vartheta = 90, \gamma = 0,\ S_c = S_r = k_p = 0.5$.

Figure 3, Figure 12 and Figure 20 portray the effect of β on the velocity profile, temperature profile and concentration profile respectively. The velocity and temperature profiles diminishes as β increases. The momentum and thermal boundary layers are diminished due to higher viscous forces as β is enhanced. In contrast, as β is magnified the concentration boundary thickens.

The role of the slope of the stretching sheet and magnetic field inclination angle is presented in Figures 4, 5, 13, 21, 22 and 23. The figures show that the thermal and velocity boundary layers decline with increasing values of ϑ and γ. The bouyancy forces decrease due to the gravity component $gcos\gamma$ which is maximal when $\gamma = 0$ i.e. when the stretching surface is vertical and is minimal when $\gamma = 90^0$. Figures 5 and 13 displays the combined effect of γ and ϑ on the temperature and velocity distribution. It is noticed that as γ and ϑ simultaneously gets smaller the temperature

Table 1: The effect of χ on the skin friction for $M = G_t = G_m = K_l = D_n = Q = R = 0,\ P_r = 1,$

χ	Mukhopadhyay *et al.*[28]	Sharidan *et al.* [38]	Mansour *et al.*[24]	Present
0.8	1.26148	1.26104	1.26150	1.26104
1.2	1.37785	1.37772	1.37713	1.37772

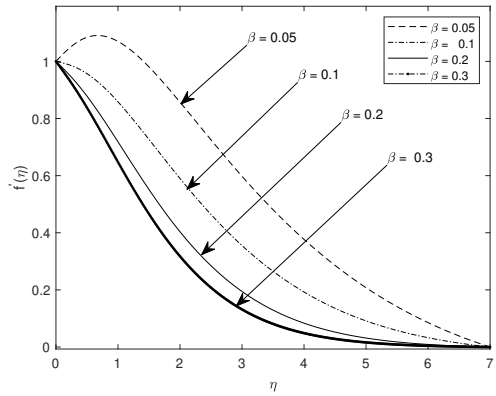

Figure 3: The effect of β on the velocity profile with $P_{ref} = 2,\ M = G_t = G_m = \chi = S_f = 1,\ \vartheta = 90, \gamma = 0,\ S_c = D_n = E_c = S_r = k_p = 0.5.$

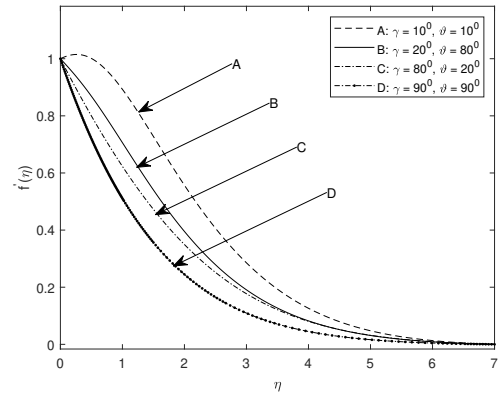

Figure 5: Combined role of ϑ and γ on the velocity distribution with $M = G_t = G_m = \chi = S_f = 1,\ S_c = D_n = E_c = S_r = k_p = 0.5,\ \beta = 0.2$ and $P_{ref} = 2.$

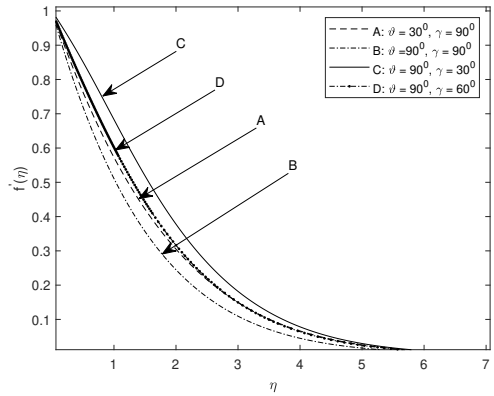

Figure 4:The effect of γ and ϑ on the velocity profile with $P_{ref} = 2,\ \beta = 0.2,\ \beta = 0.2,\ S_c = E_c = D_n = S_r = k_p = 0.5,\ M = G_t = G_m = \chi = S_f = 1.$

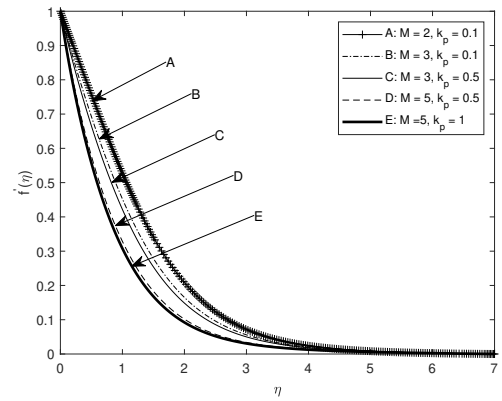

Figure 6:The influence of M and k_p on the velocity profile with $P_{ref} = 2,\ G_t = G_m = \chi = S_f = 1,\ \beta = 0.2,\ \gamma = 0, \vartheta = 90,\ D_n = E_c = S_c = S_r = 0.5.$

and velocity profiles grows. The profiles are maximal when $\gamma = \vartheta = 0$ and minimal when $\gamma = \vartheta = 90^0$. For any given combination of γ and ϑ the profiles are bigger when $\vartheta > \gamma$. On the other hand, the effect of γ and ϑ on the concentration distribution is reversed as demonstrated in Figures 21, 22 and 23. The concentration profile is enhanced with an increase in both γ and ϑ. The concentration profile achieves its maximal value when $\gamma = \vartheta = 90^0$ and achieves its minimal value when $\gamma = \vartheta = 0^0$ and for any given combination of the parameters γ and ϑ, the profile are relatively bigger when $\gamma > \vartheta$.

Figures 8, 14, 27 and 28 portrays the impact of D_n and S_r on the velocity, temperature and concentration distribution. Raising the Soret number thickens the velocity, thermal and concentration boundary layers. Physically, the Soret number upgrade results in the transport of mass to areas of higher solute concentration caused by temperature gradient. Consequently, as the molar mass diffusivity rises the concentration boundary layer thickens. The impact of increasing the Dufour parameter is to magnify the velocity and temperature profile. Conversely, the concentration profile is reduced by the increment of the Dufour parameter. The convection velocity profile is enlarged as the Dufour parameter is increased due to the effect of both the thermal and solutal concentration.

Figures 9 and 15 illustrates the impact of the effective Prandtl number on the velocity distribution and the temperature distribution respectively. Figure 9 reveals that enlargement of P_{ref} diminishes the velocity profile. On the contrary, Figure 15 reveals that enlarged P_{ref} value elevates the temperature profile provided $\eta < 0.4$ with a reversed effect for $\eta > 0.4$.

The impact of G_m, G_t and Q on velocity profile is demonstrated in Figure 7. The enhancement of each of the parameters G_m, G_t and Q grows the velocity profile. Figure 16 discloses the role of S_c, Q and E_c on the temperature distribution. The upgrade of the parameters S_c, E_c and Q enhances the temperature profile. Figures 18 and 29 depicts the role of M, G_t and G_m on the Temperature and concentration respectively. The study reveals that enlargement of the values

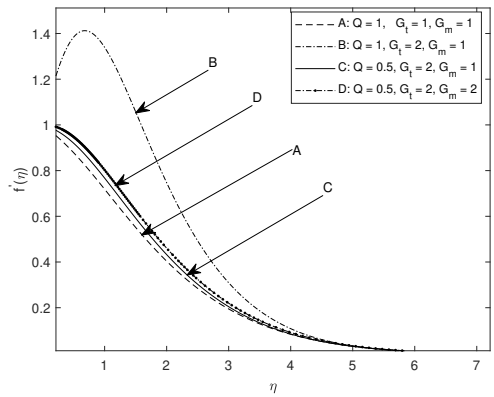

Figure 7:The influence of G_t, G_m and Q on the velocity profile with $P_{ref} = 2,\ \beta = 0.2,\ M = \chi = S_f = 1,\ \vartheta = 90, \gamma = 0,\ S_c = D_n = E_c = S_r = k_p = 0.5$.

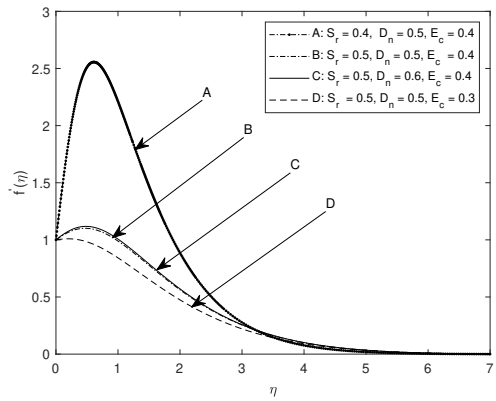

Figure 8: The effect of S_r, D_n and E_c on the velocity with $P_{ref} = 2,\ \beta = 0.2,\ M = G_t = G_m = \chi = S_f = 1,\ \vartheta = 90,\ \gamma = 0,\ S_c = S_r = k_p = 0.5$.

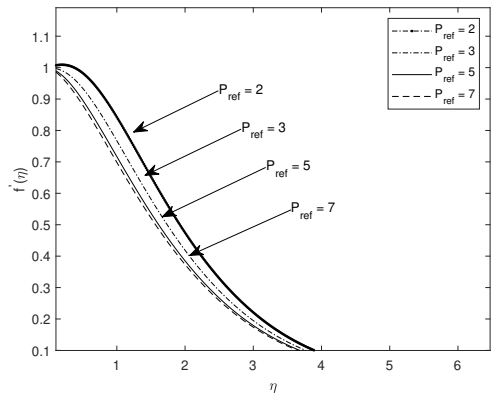

Figure 9: The effect of P_{ref} on the velocity profile with $M = G_t = G_m = \chi = S_f = 1,\ \beta = 0.2,\ \vartheta = 90, \gamma = 0,\ S_c = S_r = k_p = 0.5$.

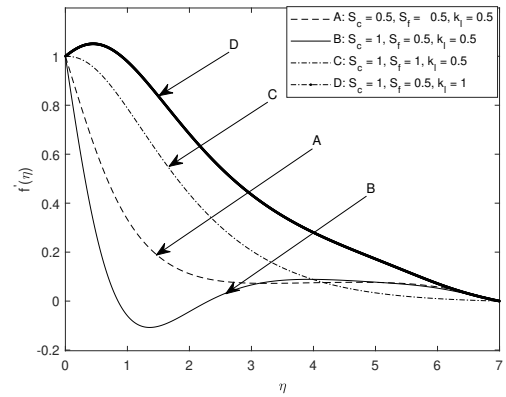

Figure 10: The influence of $S_c,\ S_f,\ k_l$ on the velocity profile with $M = G_t = G_m = \chi = 1,\ \beta = 0.2,\ \vartheta = 90, \gamma = 0,\ P_{ref} = 2,\ S_r = k_p = 0.5$.

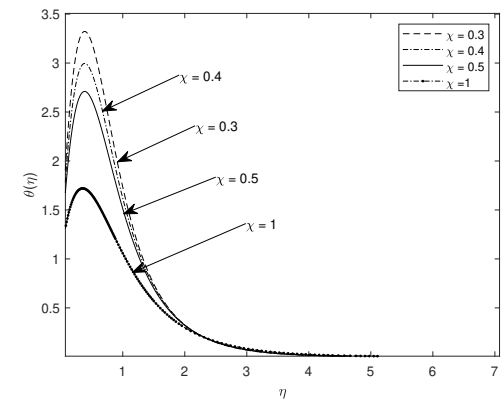

Figure 11: The effect of χ on the temperature profile with $M = G_t = G_m = S_f = 1,\ \beta = 0.2,\ \vartheta = 90, \gamma = 0,\ S_c = S_r = k_p = 0.5$.

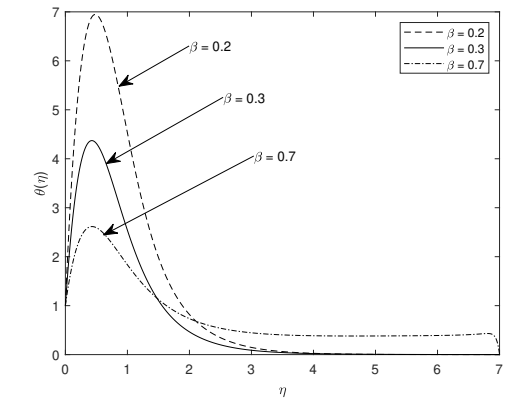

Figure 12:Temperature profile for various values of β with $M = 1,\ \vartheta = 90, \gamma = 0,\ G_t = G_m = 1,\ S_c = 0.5,\ \chi = 1,\ S_r = 0.5,\ k_p = 0.5,\ S_f = 1$.

of G_t raises the temperature profile. On the other hand, the temperature profile is lowered with the rise in the value of G_m and M. The parameters G_m and M magnifies the concentration profile close to the wall with a reversed effect further away from the wall. On the other hand, the parameter G_t has opposite effect on the concentration profile.

Figure 6 illustrates the effect of M and k_p on the velocity distribution. The graph demonstrates that the velocity profile diminishes with the rise of k_p value. The lowering of velocity is due to the reduction in the porosity tightness near the surface as k_p becomes bigger. Similar findings were reported by Das *et al.* [14]. Figure 6 also discloses that enhancement of the magnetic parameter retards fluid flow due to the Lorentz force created as a result.

It is shown that the velocity grows with the enhancement of the parameters k_l and S_f closer to the wall. On the contrary, the velocity diminishes with increasing value of S_f at free stream and S_c.

Figure 17 exhibits the effect of $k_p,\ S_f$ and k_l on the tem-

perature distribution. The figure shows that increasing values the parameter S_f and k_l diminishes the temperature distribution. Furthermore the Figure illustrates that enlarged values the parameter k_p magnifies the temperature profile.

Figure 26 depicts the impact of S_c and k_l on the concentration profile. The Figure reveals that the upgrade of the parameters S_c and k_l declines the concentration profile. Increasing the value of S_c enhances the drag effect on the concentration profile. It is demonstrated that the more the diffusing species the greater the concentration profile reduction.

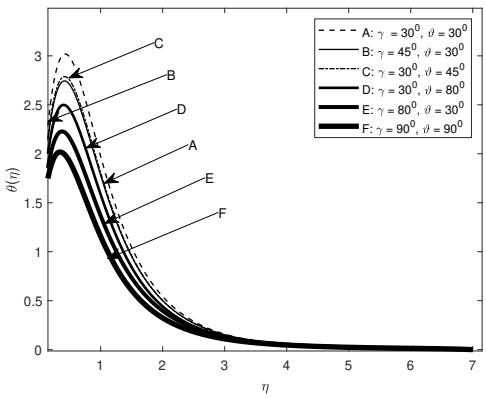

Figure 13: Combined effect of γ and ϑ on temperature profile with $M = 1,\ \beta = 0.2,\ G_t = G_m = 1,\ S_c = 0.5,\ \chi = 1,\ S_r = 0.5,\ k_p = 0.5,\ S_f = 1.$

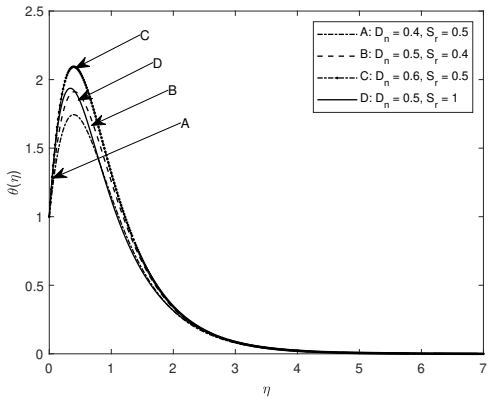

Figure 14: The influence of D_n and S_r on the temperature profile with $M = G_t = G_m = \chi = S_f = 1,\ \beta = 0.2,\ \vartheta = 90, \gamma = 0,\ S_c = k_p = 0.5.$

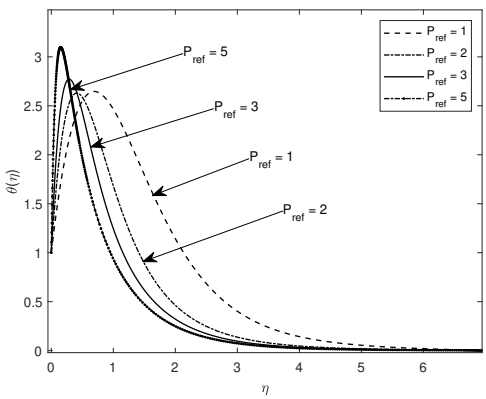

Figure 15: The influence of $Pref$ on the temperature profile with $M = G_t = G_m = \chi = S_f = 1,\ \beta = 0.2,\ \vartheta = 90, \gamma = 0,\ S_c = k_p = 0.5.$

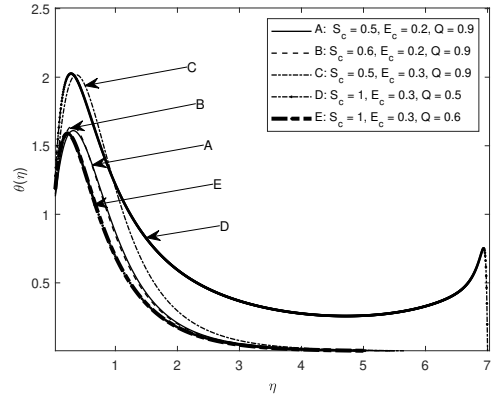

Figure 16: Temperature profile for varying values of S_c, E_c and SQ with $P_{ref} = 2,\ M = 1,\ \beta = 0.2,\ \vartheta = 90, \gamma = 0,\ G_t = G_m = 1,\ \chi = 1,\ k_p = 0.5,\ S_f = 1.$

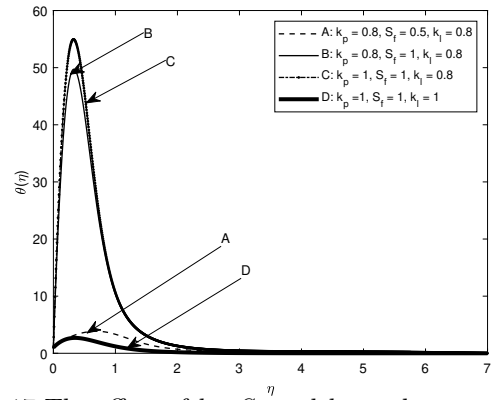

Figure 17:The effect of k_p, S_f and k_l on the temperature profile with $P_{ref} = 2,\ M = G_t = G_m = \chi = 1,\ \beta = 0.2,\ \vartheta = 90, \gamma = 0,\ \beta = 2.$

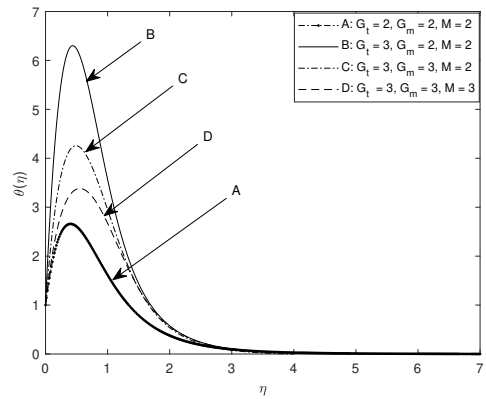

Figure 18: Temperature profile for varying values of G_t, G_m and M with $P_{ref} = 2,\ Q = 1,\ \beta = 0.2,\ \vartheta = 90, \gamma = 0,\ k_p = D_n = 0.5\ \chi = 1,\ S_f = 1.$

Also as k_l grows the rate of interfacial mass transfer is enhanced.

Figure 24 illustrates the effect of the effective Prandtl number P_{ref} and the permeability parameter k_p on the concentration distribution. Larger values of effective Prandtl number declines the concentration profile near the wall with reversed effect further away from the wall. On the other hand, the concentration profile is enhanced as the permeability parameter k_p is upgraded. The influence of $E_c,\ S_f$ and Q on the concentration is exhibited in Figure 25. The Figure reveals that increasing the value of the parameters $E_c,\ S_f$ and that

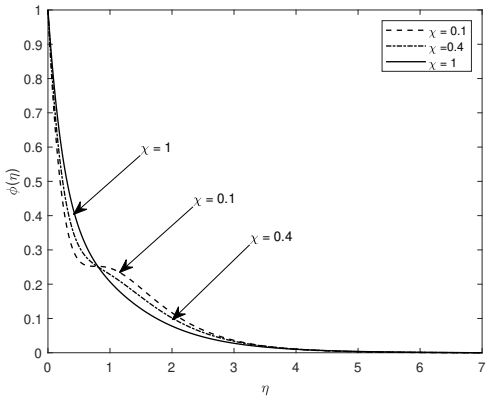

Figure 19: Concentration profile for varying values of χ with $P_{ref} = 2,\ M = 1,\ \beta = 0.3,\ \vartheta = 90, \gamma = 0,\ G_t = 3, G_m = 2,\ S_c = 0.5, S_r = 0.5,\ k_p = 1,\ k_l = 1,\ S_f = 1.$

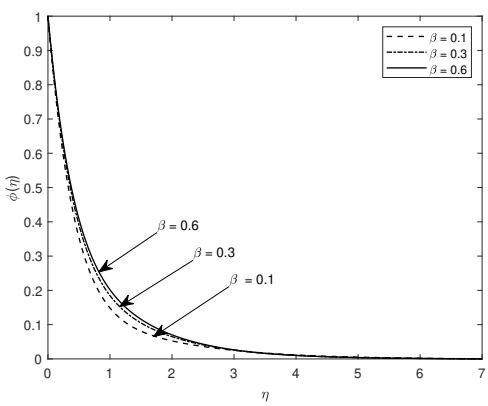

Figure 20: The effect of β on the concentration profile with $P_{ref} = 2,\ M = k_p = k_l = S_f = 1,\ \vartheta = 90, \gamma = 0,\ G_t = 3,\ G_m = 2,\ S_c = S_r = 0.5.$

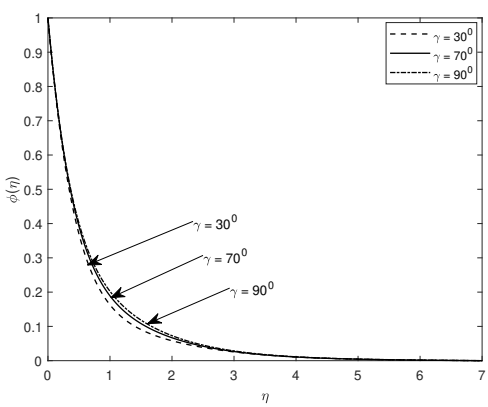

Figure 21: The effect of γ on the concentration profile with $P_{ref} = G_m = 2,\ \vartheta = 90,\ G_t = 3,\ S_c = S_r = 0.5,\ M = k_p = k_l = S_f = 1..$

of Q closer to the wall diminishes the concentration profile. It is established that further away from the wall the effect of the three parameters on the concentration profile is reversed.

The impact of the different parameters on the rate of heat transfer, rate of mass transfer and the skin friction are exhibited in Tables $2-7$. Tables $2-3$ depicts the influence of the parameters $E_c,\ S_r,\ \beta,\ P_{ref},\ \vartheta,\ \gamma,\ D_n,\ \chi,\ k_p,\ S_c,\ S_f,\ Q,\ k_l,\ G_t,\ G_m$ and M on the skin friction coefficient $f''(0)$. It is noticed that increasing any of these values causes reduction in the

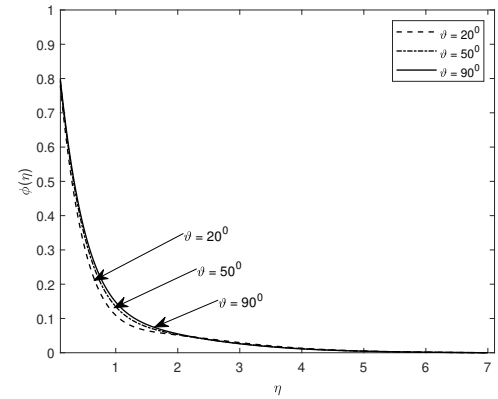

Figure 22: The effect of ϑ on the concentration profile with $G_m = P_{ref} = 2,\ M = k_p = k_l = S_f = 1,\ \gamma = 0,\ \vartheta = 90,\ G_t = 3,\ S_c = S_r = 0.5.$

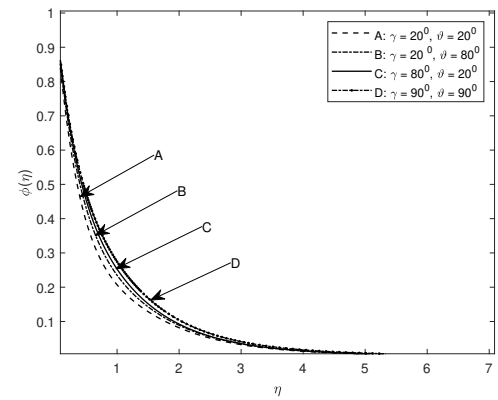

Figure 23: Combined effect of γ and ϑ on Concentration with $P_{ref} = 2,\ M = 1,\ G_t = 3, G_m = 2,\ S_c = 0.5, S_r = 0.5,\ k_p = 1,\ k_l = 1,\ S_f = 1.$

skin-friction coefficient except for $Q,\ G_t,\ G_m$ and M which manifests opposite effect. The negative wall shear stress indicates the presence of a retarding force within the flow. It is also revealed from Table $4-5$ that the heat transfer rate rises with enlarged value of $\beta,\ \chi,\ k_p,\ S_c,\ k_l,\ M$ and diminishes with increment of parameters, $S_r,\ P_{ref},\ \vartheta,\ \gamma,\ D_n,\ S_f,$ and Q. The role of the different parameters on the rate of mass transfer is displayed in Tables 6 and 7. We infer that, the rate of mass transfer is elevated as $S_r,\ S_c,\ k_l,\ k_p,\ \vartheta,\ M$ and Q increases and declines with upgrade of each of the parameters, $P_{ref},\ \beta,\ \gamma,\ D_n,\ \chi,\ S_f$ and E_c. The parameters G_t and G_m have no effect on the mass transfer rate.

V. CONCLUDING REMARKS

The present paper analyzes the effect of the effective Prandtl number, surface slope, aligned magnetic field and heat generation on the MHD Casson fluid. The governing PDE's are converted to non-linear ODE's by using suitable similarity transformations. The results of the investigation are presented in the form of tables and graphs. The outcome of the numerical study are stated as follows:

1. Upgrade in the values of G_t,G_m, Q, D_n, S_f, k_l and S_r enhances the velocity and decreases with the increase in the value of χ, M, ϑ, γ, β, k_p, S_c and P_{ref}.
2. The temperature distribution grows with enlargement of parameters Q, D_n, S_r, S_c, E_c, G_t, k_p, $P_{ref} < 0.4$ closer to the wall and diminishes with increase in the value of

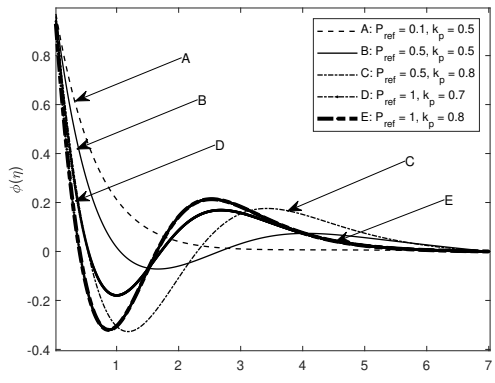

Figure 24: Effect of P_{ref} and k_p on concentration profile with $M = 1,\ \beta = 0.2,\ G_t = G_m = 1,\ S_c = 0.5,\ \chi = 1,\ S_r = 0.5,\ S_f = 1.$

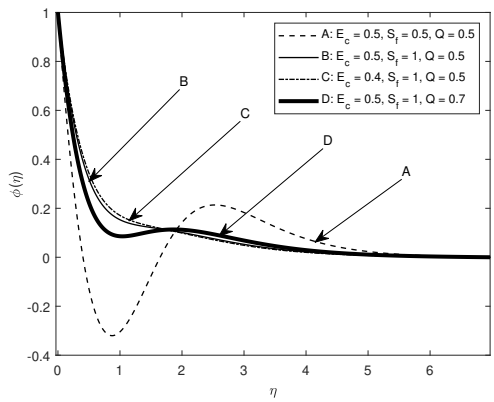

Figure 25: Effect of S_f, E_c and Q on concentration profile with $M = 1,\ \beta = 0.2,\ G_t = G_m = 1,\ S_c = 0.5,\ \chi = 1,\ S_r = 0.5.$

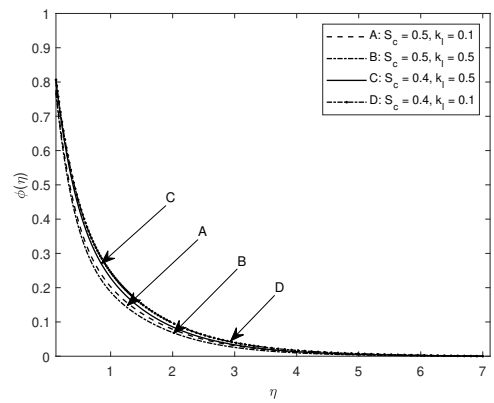

Figure 26: The influence of S_c and k_l on the concentration profile with $G_m = P_{ref} = 2,\ M = k + p = S_f = 1,\ \vartheta = 90,\ \gamma = 0,\ S_r = 0.5.$

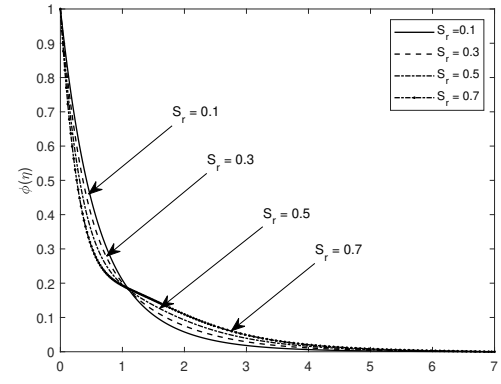

Figure 27: The effect of S_r on the concentration profile with $P_{ref} = G_m = 2,\ M = k_p = k_l = S_f = 1,\ \vartheta = 90,\ G_t = 3,\ S_c = 0.5.$

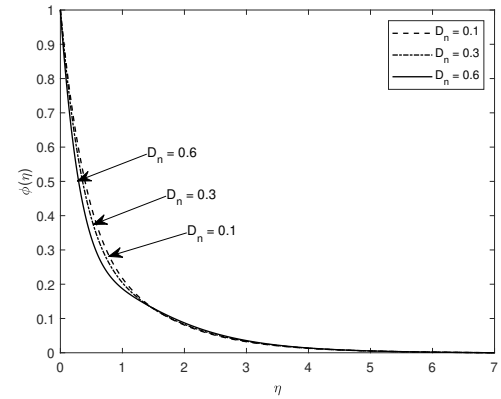

Figure 28: The effect of D_n on the concentration profile with $G_m = P_{ref} = 2,\ \vartheta = 90,\ G_t = 3,\ S_c = S_r = 0.5,\ M = k_p = k_l = S_f = 1.$

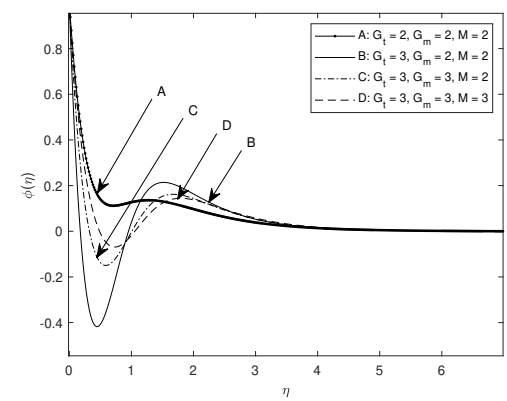

Figure 29: The influence of $G_t,\ G_m$ and M on the concentration profile with $P_{ref} = 2,\ k_p = k_l = S_f = 1,\ S_c = S_r = 0.5,\ \vartheta = 90,\ \gamma = 0.$

χ, ϑ, γ, β, S_f, G_m, M, k_l and $P_{ref} > 0.4$ further away from the wall.

3. The concentration profile grows as $\beta,\ \gamma,\ \vartheta,\ S_f,\ G_m,\ M$ and S_r and declines with the rise in the value of $\chi,\ D_n,\ S_c,\ E_c,\ Q,\ P_{ref},\ k_p,\ G_t$ and k_l.
4. The velocity and temperature profiles are enhanced as γ and ϑ gets smaller and the profiles are maximal when $\gamma = \vartheta = 0$ and minimal when $\gamma = \vartheta = 90^0$. For any given combination of γ and ϑ the velocity and temperature profiles are bigger when $\vartheta > \gamma$. The parameters, γ and ϑ have opposite effect on the concentration profile. The concentration profile achieves maximal values when $\gamma = \vartheta = 90^0$ and minimal when $\gamma = \vartheta = 0^0$ and for any combination of γ and ϑ the profile is bigger when $\gamma > \vartheta$.
5. Growing the value of the parameters $E_c,\ S_r,\ \beta,\ P_{ref},\ \vartheta,\ \gamma,\ D_n,\ k_p,\ S_c,\ S_f,\ k_l$ and χ diminishes the skin friction coefficient. Conversely, the skin friction rises with increasing value of $Q,\ G_t,\ G_m$ and M.
6. The rate of heat transfer rises with increasing values of the parameters $E_c,\ k_p,\ S_c,\ k_l,\ M$ and diminishes with increasing value of $S_r,\ \beta,\ P_{ref},\ \vartheta,\ \gamma,\ D_n,\ S_f,\ G_t,\ G_m$

Table 2: The effect of E_c, Sr, ϑ, γ, P_{ref}, β, D_n and χ on the skin friction coefficient $f''(0)$ with $G_t = G_m = Q = S_c = M = k_p = k_l = S_f = 1$

E_c	S_r	β	P_{ref}	ϑ	γ	D_n	χ	$f''(0)$
0.5	0.1	0.5	1	90	0	1	1	-0.4432
0.4								-0.4773
0.1								-1.1844
2	0.3							-0.9961
	0.5							-1.1352
	0.9							-1.5319
		0.7						-0.7919
		1						-0.8797
			3					-1.2391
			5					-4.9434
				30				-0.4539
				60				-1.7329
					30			-0.7812
					60			-1.3562
						2		-0.6692
						3		-2.9791
							0.4	-1.6706
							0.9	-2.4570
							0.1	-1.5152

Table 3: The influence of k_p, S_c, Q, S_f, k_l and M on the skin friction coefficient $f''(0)$ with $G_t = G_m = P_{ref} = D_n = 1$ and $E_c = 0.5$

k_p	S_c	Q	S_f	k_l	G_t	G_m	M	$f''(0)$
0.5	0.5	0.5	0.5	0.5	1	1	1	-0.2206
0.7								-0.2900
0.9								-0.3537
	0.4							-0.3437
	0.3							-0.3312
	0.2							-0.3133
		0.1						-0.4192
		0.4						-0.3521
		0.6						-0.2530
			0.8					-0.4005
			0.9					-0.4395
			1					-0.4761
				0.6				-0.4776
				0.7				-0.4790
				0.9				-0.4817
					2			0.5824
					3			0.9564
					5			1.0760
						2		0.2981
						3		0.4016
						5		0.8849
							2	1.0580
							3	1.3569

Table 4: Influence of Sr, ϑ, γ, P_{ref}, β, D_n, χ and Q on the rate of heat transfer $-\theta'(0)$ with $G_t = G_m = S_c = M = k_p = K_l = S_f = 1$, $E_c = 0.5$

S_r	β	P_{ref}	ϑ	γ	D_n	χ	Q	$-\theta'(0)$
0.4	0.5	1	90	0	1	1	1	13.929
0.6								9.6917
0.7								6.3938
	0.7							9.3839
	1							9.5357
		5						5.5066
		7						5.0698
		10						2.9811
			30					4.0654
			60					3.9932
				30				10.8003
				50				0.9582
				60				0.4765
					2			3.9519
					3			3.6124
						0.8		4.6987
						0.5		3.6499
						0.1		3.1471
							0.1	3.4334
							0.4	3.2802
							0.8	3.1793

Table 5: Influence of k_p, S_c, S_f, k_l, G_t, G_m, M on the heat transfer rate $-\theta'(0)$ with $D_n = S_r = Q = 1$ and $\beta = E_c = 0.5$

k_p	S_c	S_f	k_l	G_t	G_m	M	$-\theta'(0)$
0.5	0.5	0.5	0.5	1	1	1	-25.190
0.7							4.6956
0.9							4.6958
	0.4						1.7054
	0.3						1.2516
	0.2						-3.4786
		0.4					11.538
		0.8					7.4522
		0.9					5.0080
			0.6				5.0080
			0.7				5.0146
			0.9				5.0276
				2			-3.5663
				4			-12.140
					2		5.9750
					3		3.0368
					5		-40.390
						3	-52.116
						4	0.6795
						5	2.4725

and χ.

7. The rate of mass transfer is enhanced with the upgrade of the parameters S_c, S_r, k_l, ϑ, k_p, M and Q and is reduced with improved value of P_{ref}, β, γ, D_n, χ, S_f and E_c. The role of the parameters G_t and G_m on the rate of mass transfer is insignificant.

The outcome of our investigation on the influence of the different parameters on the fluid flow agrees with previous publications. The outstanding findings in the present study are that raising value of the effective Prandtl number enhances the temperature profile $\eta < 0.4$ and velocity profile whereas the concentration profile diminishes. Also, the enlargement of γ and ϑ diminishes the temperature and velocity distribution whereas the

Table 6: The effect of $S_r,\ S_c,\ P_{ref},\ \beta,\ D_n,\ k_l,\ E_c$ on the mass transfer rate $-\phi'(0)$ with $G_t = G_m = S_c = M = k_p = S_f = \chi = 1,\ \gamma = 0,\ \vartheta = 90$.

S_r	S_c	P_{ref}	β	k_l	E_c	D_n	$-\phi'(0)$
0.3	0.5	1	0.5	1	0.5	1	1.7831
0.5							2.7957
1							4.7430
	0.2						1.7402
	0.3						2.5373
	0.5						4.7430
		1					4.7430
		5					4.5230
		10					0.6882
			0.3				1.5384
			0.4				0.8118
			0.9				0.6531
				0.6			0.2190
				0.7			0.3825
				0.9			0.6548
					0.3		0.8148
					0.4		0.7040
					0.5		0.6548
						1	0.7040
						2	0.6970
						4	0.6303

Table 7: The influence of $\vartheta,\ \gamma,\ \chi,\ k_p,\ Q,\ S_f$ and M on the mass transfer rate $-\phi'(0)$ with $S_c = E_c = 0.5,\ \beta = k_l = 0.9,\ D_n = 4,\ S_r = 1$ and $P_{ref} = 10$.

γ	ϑ	χ	k_p	Q	S_f	M	G_t	G_m	-$\phi'(0)$
45	90	1	0.5	0.5	0.5	1	1	1	2.6239
80									-0.1458
90									-0.1995
	60								-0.2284
	30								-0.3014
	0.1								-0.3932
		0.2							-0.4167
		0.3							-0.4441
			0.7						-0.4335
			0.8						-0.4284
			1						-0.4185
				0.6					-0.4068
				0.8					-0.3902
				1					-0.3778
					0.6				-0.4074
					0.8				-0.4650
						1			-0.5211
						2			0.4616
						3			0.4236
						4			0.3872
							2		0.3872
							3		0.3872
							5		0.3872
								2	0.3872
								3	0.3872
								5	0.3872

concentration profile is is elevated. For optimal velocity and temperature profiles the angles $\vartheta = \gamma = 0$ and for any given combination of the inclination angles, $\vartheta \geq \gamma$. On the other hand, the concentration profile is optimal when $\gamma = \vartheta = 90^0$ and for any given combination of the inclination angles, $\gamma > \vartheta$. centering

REFERENCES

[1] N. Acharya, S. Maity, and P. K. Kundu, "Influence of inclined magnetic field on the flow of condensed nanomaterial over a slipping surface:the hybrid visualization", Applied Nanoscience, vol. 10, pp. 633-647, 2020.

[2] M S. Alam, M. N. Rahman and A. Satter, "Effects of variable suction and thermophoresis on steady MHD combined free-forced convective heat and mass transfer flow over a semi-infinite permeable inclined plate in the presence of thermal radiation", Int. J. Therm. Sci., vol. 47, no. 6, pp. 758-765, 2008.

[3] M. S. Alam, M. M. Rahman, and A. Satter, "Transient magnetohydrodynamic free convective heat and mass transfer flow with thermophoresis past a radiate inclined permeable plate in the presence of variable chemical reaction and temperature dependent viscosity", Nonlinear Analysis: Model Control, vol. 14, pp. 3-20, 2009.

[4] C. R. A. Abreu, M. F. Alfradique, A. S. Telles, "Boundary layer flows with Dufour and Soret effects:I:forced and natural convection". Chem. Eng. Sci., vol. 61, no. 13, pp. 4282-4289, 2006.

[5] A. I. L. Animasaun, "Effects of thermophoresis, variable viscosity and thermal conductivity on free convective heat and mass transfer of non-Darcian MHD dissipative Casson fluid flow with suction and nth order of chemical reaction", J. Niger. Math. Soc., vol. 34, no. 1, pp. 11-31, 2015.

[6] K. K. Asongwa, and A. A. Ibe, "A study of MHD Casson fluid flow over a permeable stretching sheets with heat and mass transfer", Journal of Engineering Research and Reports, vol. 16, no. 2, pp. 10-25, 2020.

[7] K. Bhattacharya, T. Hayat, and A. Alsaedi, "Analytic solution for magnetohydrodynamic boundary layer flow of Casson fluid over a stretching/shrinking sheet with wall mass transfer", Chinese Physics B, vol. 22, no. 2, pp. 6, doi:101088/1674-1056/22/2/024702, 2013.

[8] K. Bhattacharya, T. Hayat, and A. Alsaedi, "Exact solution for boundary layer flow of Casson fluid over a permeable stretching /shrinking sheet", Z. Angew. Math., vol. 94, pp. 522-528, 2014.

[9] G. Buzuzi, J. B. Munyakazi, and K. C. Patidar, "A fitted numerical method to investigate the effect of various parameters on an MHD flow over an inclined plate", Numer. Methods for Partial Diff. Equations, pp. 107-120, DOI 10.1002/num, 2015.

[10] G. Buzuzi and A. N. Buzuzi, "Unsteady MHD convection flow and heat transfer past a vertical inclined plate in a porous medium with variable plate temperature with suction in a slip flow regime", Int. J. of Appl. Math., vol. 32, no. 2, pp. 205-218; DOI: 10.12732/ijam.v32i2.4, 2019.

[11] G. Buzuzi, G. Makanda, "Numerical analysis on unsteady MHD flow and heat transfer over an inclined

stretching surface in a porous medium with heat source and variable magnetic field angle", International Journal of Applied Mathematics, vol. 35, no. 2, pp. 205-223, 2022.

[12] G. Buzuzi, A. N. Buzuzi, T. Nyamayaro, W. Manamela and K. S. Ramolotja, "The study of magneto hydrodynamic free convective flow and heat transfer in a porous medium with heat generation, radiation absorption and chemical reaction", Int. J. of Appl. Math., vol. 33, no. 4, pp. 733-756, DOI: 10.12732/ijam.v33i4.15, 2020.

[13] G. Buzuzi, "Inclined magnetic field and effective Prandtl number effects on unsteady MHD oscillatory flow past an inclined surface with constant suction and chemical reaction", Journal of the Nigerian mathematical Society, vol. 40, no. 3, 227-244, 2021.

[14] M. Das, G. Mahanta, S. B. Parida, and R. Nandkeolyar," Hydromagnetic flow of a heat radiating chemically reactive Casson nanofluid past a stretching sheet with convective boundary conditions" In: R. Sharma (Ed.), AIP Conference Proceedings, vol. 1975, no. 1, Himachal Pradesh: AIP Publishing: 030015, 2018.

[15] M. Das, G. Mahanta, S. Shaw, and S. B. Parida, "Unsteady MHD chemically reactive double-diffusive Casson fluid past a flat plate in porous medium with heat and mass transfer", Heat Transfer-Asian Res., vol. 48, pp. 1761-1777, 2019.

[16] S. S. Das, A. Satapathy, J. K. Das and J. P. Panda, "Mass transfer effects on MHD flow and heat transfer past a vertical porous plate through a porous medium under oscillatory suction and heat souces", International Journal of Heat and Mass Transfer, vol 52, pp. 5962-5969, 2009.

[17] N S. Elgazery, "The effects of chemical reaction, Hall and ion-slip currents on MHD fow with temperature dependent viscosity and thermal diffusivity", Communications in Nonlinear Science and Numerical Simulations, vol. 14, no. 4, pp. 1267-1283, 2009.

[18] D. Gopal, N. Kishan, and C. S. K. Raju, "Viscous and Joule's dissipation on Casson fluid over a chemically reacting stretching sheet with inclined magnetic field and multiple slips", Inf Med Unlocked, vol. 9, pp. 154-160, 2017.

[19] G. Gurran, K. S. Dalamarugan, V. C. C. Raju, and N. Vedavathi, "Effect of chemical reaction on MHD Casson fluid flow past an inclined surface with radiation", Skit Research Journal, vol. 7, no. 1, pp. 53-59, 2007.

[20] S. Jain, and M. Kumari, "Inclined MHD Casson fluid flow over a permeable cylinder with viscous dissipation and chemical reaction", International Journal of Mathematical Sciences, vol. 17, pp. 205-226, 2018.

[21] Y. O. Koroleva, A. V. Korolev, "Effect of vessel roughness in Casson's mathematical model of blood flow", IAENG International Journal of Applied Mathematics, vol. 50, no. 2, pp. 405-408, 2020.

[22] C. P. Kumar, K. Raghunath, and M. Obulesu, "Thermal diffusion and inclined magnetic field effects on MHD free convection flow of Casson fluid past an inclined plate in conducting field", Turkish Journal of Computer and Mathematics Education, vol. 12, no. 13, pp. 960-977, 2021.

[23] F. S. Ibrahim, A. M. Elaiw and A. A. Bakr, "Effect of the chemical reaction and radiation absorption on the unsteady MHD free convection flow past a semi infinite vertical permeable moving plate with heat source and suction", Commun. in Nonlin. Sci. and Numer. Simul., vol. 13, pp. 1056-1066, 2008.

[24] M. A. Mansour, A. E. S. M. Mahdy, and S. E. Ahmed, "Entropy analysis for unsteady MHD boundary layer flow and heat transfer of Casson fluid over a stretching sheet", Walailak Journal of Science and Technology, vol. 14, no. 2, pp. 169-187, 2017.

[25] E. Mgyari, "Comment on " Mixed convection boundary layer flow over a horizontal plate with thermal radiation by A Ishak, Heat mass Transfer, DOI 10.1007/s00231-009-0552-3", Heat Mass Transfer, vol. 46, pp. 509-810, 2010.

[26] E. Magyari, and A. Pantokratoras, "Note on the effect of thermal radiation in the linearized Roseland approximation on the heat transfer characteristics of various boundary layer flows", International Communications in Heat and Mass Transfer, vol. 38, pp. 554-556, 2011.

[27] S. Mukhopadhyay, "Casson fluid flow and heat transfer over a non linearly stretching surface", Chinese Physics B, vol. 22, no. 7, pp. 074701-5, 2013.

[28] S. Mukhopandhyay, D. R. Prativa, K. Bhattacharya, and G. C. Klayek, "Casson flow over an unsteady stretching surface", Ain Shams Eng. J., vol. 4, pp. 933-938, 2013.

[29] S. Nadeem, R. U. Haq, and C. Lee, "MHD flow of a Casson fluid over an exponentially shrinking sheet", Scientia Iranica, vol. 19, pp. 1550-1553, 2012.

[30] S. Nadeem, M. Rashid, and N. S. Akbar, "Optimized analytical solution for oblique flow of a Casson nano fluid with convective boundary conditions", Int. J. Therm. Sci., vol. 78, pp. 90-100, 2014.

[31] S. Pramanik, "Casson fluid flow and heat transfer past an exponentially porous stretching surface in presence of thermal radiation", Ain Shams Eng. J., vol. 5, pp. 205-212, 2014.

[32] K. Rafique, M. I. Misiran, I. Khan, S. O. Alharbi, P. Thounthong, and K. S. Nisar, "Numerical solution of Casson nanofluid flow over a non-linear inclined surface with Soret and Dufour effects by Keller-method", Frontier in Physics, vol. 7, no. 139, pp. 1-13, 2019.

[33] C. S. K. Raju, N. Sandeep, C. Sulochana, V. Sugunamma and M. Jayachandra, "Radiation, inclined magnetic field and cross-diffusion effects on flow over a stretching surface", Journal of the Nigerian Mathematical Society, vol. 34, pp. 169-180, 2015.

[34] G. S. Reddy, S. K. Reddy, P. D. Prasad, and S. V. Varma, "Diffusion-thermo and aligned magnetic field effects on force convection on flow past an inclined porous plate with first order chemical reaction", IOSR Journal of Electrical and Electronics Engineering, Vol. 12, no. 3, pp. 325-33, 2017.

[35] P. Roja, T. S. Reddy and N. B. Reddy, "Double diffusive convection-radiation interaction on unsteady Mhd flow of a micropolar fluid over a vertical moving porous plate embedded in a porous medium with

heat generation and soret effects", Int. J. of Engin. and Sci., vol. 1, no. 2, pp. 201-214, 2012.

[36] S. O. Salawu and M. S. Dada, "Radiation heat transfer of variable viscosity and thermal conductivity effects on inclined magnetic field with dissipation in a non-Darcy medium", Journal of the Nigerian mathematical Society, vol. 35, pp. 93-106, 2016.

[37] N. Sandeep and V. Sugunamma, "Radiation and inclined magnetic field effects on unsteady hydromagnetic free convection flow past an impulsively moving vertical plate in a porous medium", J. Appl. Fluid. Mech, vol. 7, no. 2, pp. 275-286, 2014.

[38] S. Sharidan, T. Mahmood, I. Pop, "Similarity solutions for the unsteady boundary layer flow and heat transfer due to a stretching sheet", International Journal of Mechanics and Engineering, vol. 11, no. 3, pp. 647-654, 2006.

[39] M. A. Seddeek, and M. S. Abdelmeguid, "Effects of radiation and thermal diffusivity on heat transfer over a stretching surface with variable heat flux", Physics Letters A, vol. 348, no. 36, pp. 172-179, 2006.

[40] S. Shateyi, S. S. Motsa, and P. Sibanda, "The effects of Thermal Radiation, Hall currents, Soret, and Dufour on MHD Flow by Mixed Convection Over a Vertical Surface in Porous media", Mathematical Problems in Engineering, vol 2010, Article ID 627475, 20 pages, 2010.

[41] C. Sivaraj, and M. A. Sheremet, "MHD natural convection in an inclined square porous cavity with a heat conducting solid block", Journal of Magnetism and Magnetic materials, vol. 426, pp. 351-360, 2017.

[42] M. J. Uddin, "Convective flow of micropolar fluids along an inclined flat plate with variable electric conductivity and uniform surface heat flux", DAFFODIL Int. Univ. J. of Sci. and Techn., Vol. 6, no. 1, pp. 69-79, 2011.

[43] I. Ullah, S. Shafie, and I. Khan, "Effects of slip condition and Newtonian heating on MHD flow of Casson fluid over a nonlinearly stretching sheet saturated in a porous medium", J. king Said Univ-Sci. vol. 29, no. 2, pp. 250-259, 2017.